Title
Ascending Columns, WTG, and Convective Aggregation

Journal
Journal of the Atmospheric Sciences, 78(2)

ISSN
0022-4928

Author
Romps, David M

Publication Date
2021-02-01

DOI
10.1175/jas-d-20-0041.1

Peer reviewed

Ascending Columns, WTG, and Convective Aggregation

DAVID M. ROMPS[a,b]

[a] *Department of Earth and Planetary Science, University of California, Berkeley, Berkeley, California*
[b] *Climate and Ecosystem Sciences Division, Lawrence Berkeley National Laboratory, Berkeley, California*

(Manuscript received 10 February 2020, in final form 26 September 2020)

ABSTRACT: Analytic solutions are derived for a convecting atmosphere with mean ascent using a zero-buoyancy bulk-plume approximation for moist convection. It has been suggested that such solutions should serve as a model for the relationship between humidity, instability, and precipitation in the tropics, but it is shown here that this interpretation is incompatible with the observed weak temperature gradient (WTG). Instead, the solutions can be used to understand the atmospheric state averaged over all tropical convecting regions. Using the analytic solutions in this way, they predict the changes in humidity, instability, and precipitation as a function of the size of the moist patch in a convectively aggregated state.

KEYWORDS: Convection; Radiative-convective equilibrium

1. Introduction

In recent years, there has been substantial progress in understanding the structure of radiative–convective equilibrium (RCE). This progress was sparked by Singh and O'Gorman (2013), which introduced the zero-buoyancy approximation for convective plumes. In this approximation, convection is treated as having the same temperature as its surrounding environment. This approximation is clearly inadequate for understanding the dynamics of convection, but its use for understanding atmospheric stratification can be justified by the fact that typical cloud buoyancies in the tropics are less than 1 K (Lawson and Cooper 1990; Romps 2010; Sherwood et al. 2013; Romps and Charn 2015). The implication of the zero-buoyancy approximation for RCE is that the mean convective available potential energy (CAPE) is related to the mean saturation deficit of the free troposphere because the saturation deficit affects entraining clouds, which, in turn, set the mean lapse rate. This idea was validated in a series of cloud-resolving experiments (Singh and O'Gorman 2013; Seeley and Romps 2015, 2016).

The zero-buoyancy approximation has also been used to derive analytic solutions for RCE's relative humidity (RH) and lapse rate, and to show that RH is, to good approximation, an invariant function of temperature in the tropical troposphere (Romps 2014). This latter result that has been shown to hold in global climate models (Po-Chedley et al. 2019) and has been used to explain the $\sim$2% K^{-1} increase in global precipitation rate (Jeevanjee and Romps 2018). Furthermore, Romps (2016) showed that the solutions of Romps (2014) could be integrated in height (with a particular choice of entrainment rate) to give an analytic expression for CAPE.

All of this progress has been in the context of RCE, but the tropical atmosphere has large-scale circulations with regions of ascent (e.g., the ITCZ) and descent (e.g., the subtropics). To understand how these large-scale circulations affect relative humidity and static stability, the solutions of Romps (2014) need to be generalized to allow for a nonzero net mass flux. An attempt at this was made by Singh et al. (2019), but, as shown here, that work contained two errors: an error of mathematics and an error of interpretation. Regarding the latter, Singh et al. (2019) interpreted their solutions as a useful framework for understanding the *covariation* of RH, CAPE, lapse rate, and precipitation in the tropics, but it will be argued here that this is not a correct interpretation. Instead, the solutions provide insight into the *mean* properties of tropical convecting regions, the stability of the tropics as a whole, and the state of convective aggregation in numerical models. In the sections that follow, the bulk-plume and zero-buoyancy approximations are used to extend the analytic RCE solutions of Romps (2014) to include net vertical motion and to explore their implications.

2. Derivation

RCE may be thought of as the steady-state solution of an atmosphere in a box: we control the radiative heating rate Q ($W\,m^{-3}$), either by specifying it directly or by choosing a radiation scheme, and there are fluxes of sensible heat and water that pass through the floor, but the faces of the box are otherwise impermeable to air, heat, and water. For a non-RCE atmosphere, we may vent the walls of the box, forcing air to enter or exit the sides of the box at each height. In general, this will cause there to be a nonzero net vertical mass flux M ($kg\,m^{-2}\,s^{-1}$) at a range of heights in the box. The steady state of such an atmosphere might appropriately be called radiative–convective–advective equilibrium (RCAE), with "advective" referring to the net vertical advection of mass, momentum, and energy.[1] Since we control the ventilation on the sides of the box, M at each height is a parameter that, like Q, may be controlled externally.

[1] Warren et al. (2020) have used the term RCDE with "D" standing for "dynamical."

Corresponding author: David M. Romps, romps@berkeley.edu

DOI: 10.1175/JAS-D-20-0041.1

We will focus on solutions at a single height in an RCAE atmosphere. Those solutions can be integrated numerically to obtain full profiles within the box as in Romps (2014), but we will not do so here. All of the points we wish to make in this paper can be understood from studying the solutions at a single height. Therefore, from here on, Q and M will refer to the radiative heating and net mass flux at a chosen height in the box with temperature T and pressure p.

To model the atmosphere within the box, we will use the bulk-plume approximation. Borrowing from the notation of Romps (2020), we will denote the upward mass flux in clouds as M_c and the upward mass flux in the environment as M_e (note that the value of M_e will be negative). The net mass flux M is equal to the sum of these: $M = M_c + M_e$. Using the notation of Singh et al. (2019), we will define $r \equiv -M_e/M_c$ as the ratio of the magnitudes of the descending environmental mass flux and the ascending cloud mass flux [note that M_e here is equal and opposite to the M_d variable of Singh et al. (2019)].

To represent the convergence of air through the sides of the box, we will denote the large-scale horizontal convergence of mass by l (kg m^{-3} s^{-1}). Then, the steady-state bulk-plume equations for mass, water, and moist static energy (MSE) are

$$\frac{\partial}{\partial z}M_c = e - d, \tag{1}$$

$$\frac{\partial}{\partial z}M_e = d - e + l, \tag{2}$$

$$\frac{\partial}{\partial z}(M_c q_v^*) = eq_v - dq_v^* - c, \tag{3}$$

$$\frac{\partial}{\partial z}(M_e q_v) = dq_v^* - eq_v + lq_v, \tag{4}$$

$$\frac{\partial}{\partial z}(M_c h^*) = eh - dh^*, \tag{5}$$

$$\frac{\partial}{\partial z}(M_e h) = dh^* - eh + lh + Q. \tag{6}$$

Here, e and d (kg m^{-3} s^{-1}) are the rates of entrainment and detrainment, respectively. The mass fraction of water vapor in the environment is q_v (kg kg^{-1}) and the mass fraction of water vapor in the convection is q_v^*, with an asterisk to denote that this is the saturated value. In these equations, we have used the zero-buoyancy approximation, as introduced by Singh and O'Gorman (2013) and used by Romps (2014); under this approximation, the small virtual effect is ignored and the temperatures of the convection and environment are treated as equal at the same height. MSE is represented in these equations by h (J kg^{-1}), with $h = c_pT + gz + Lq_v$ being the value in the environment and $h^* = c_pT + gz + Lq_v^*$ being the value in the convection. Here, L is the latent heat of evaporation, c_p is the specific heat capacity of air at constant pressure, and g is the gravitational acceleration. In Eq. (3), c is the condensation rate (W m^{-3}). Note that, in Eqs. (5) and (6), the radiative heating rate Q (which will be negative to give cooling) is applied only to the environment since the clouds are assumed to occupy a negligible fractional area; equivalently, clouds rise too quickly for radiative cooling to be of any practical relevance to their energy budget. Note also that horizontal convergence has been included in these equations, but not horizontal advection. Finally, we have simplified matters by assuming a precipitation efficiency of one; i.e., condensates fall out as rain without any evaporation in the environment. This same simplification was used in sections 1–5 of Romps (2014) and in section 2.3 of Singh et al. (2019).

Our first task is to derive an expression for the environmental mass flux. The mathematical error of Singh et al. (2019) was to assume that "the downward mass flux in the environment remains fixed at its RCE value irrespective of the upward mass flux in the [convection]," an approximation that was claimed to be "valid if it may be assumed that the downward mass flux is set by a balance between radiative cooling and subsidence in the environment and that the radiative cooling rate itself is fixed." To see why this is not a valid assumption, we can subtract L times (4) from (6) and then use (2) to obtain

$$M_e = \frac{Q}{g - c_p\Gamma}. \tag{7}$$

In the solution below, we will see that Γ varies from the dry lapse rate to the moist lapse rate as the net mass flux is varied, leading to dramatic variations in M_e.

Equations (1)–(6) can be solved analytically in terms of M and Q (and also the chosen p, T, e, and d) and the derivation and solutions are given in the appendix. In RCE (i.e., $M = 0$), the cloud mass flux and condensation rate are

$$M_{c,\mathrm{RCE}} = -\frac{C}{Lq_v^*}Q, \tag{8}$$

$$c_{\mathrm{RCE}} = -\frac{1}{L}Q, \tag{9}$$

where the constant C (constant in the sense that it does not depend on M or Q) is defined in Eq. (A36). Note that both $M_{c,\mathrm{RCE}}$ and c_{RCE} are linear in the radiative heating rate Q (which, as we recall, is negative). Note also that c_{RCE} does not depend at all on the rates of entrainment or detrainment; in the absence of any large-scale flow, the condensation rate must balance the radiative cooling. Figure 1 shows the dependence of $M_{c,\mathrm{RCE}}$ and c_{RCE} on the fractional entrainment rate ($\varepsilon \equiv e/M_c$) and the fractional detrainment rate ($\delta \equiv d/M_c$). Figure 1 supplements Fig. 2 of Romps (2014), which plotted $\mathrm{RH}_{\mathrm{RCE}}$ as a function of ε and δ.

For the general solution (i.e., for any net mass flux M), it is helpful to define

$$\tilde{c} \equiv c/c_{\mathrm{RCE}}, \tag{10}$$

$$\tilde{M} \equiv M/M_{c,\mathrm{RCE}}, \tag{11}$$

$$\tilde{M}_c \equiv M_c/M_{c,\mathrm{RCE}}, \tag{12}$$

$$\tilde{M}_e \equiv M_e/M_{c,\mathrm{RCE}}, \tag{13}$$

so that $\tilde{c}$ is the condensation rate normalized by its RCE value, and $\tilde{M}$, $\tilde{M}_c$, and $\tilde{M}_e$ are the net, cloud, and environmental mass fluxes, respectively, all normalized by the cloud mass flux in

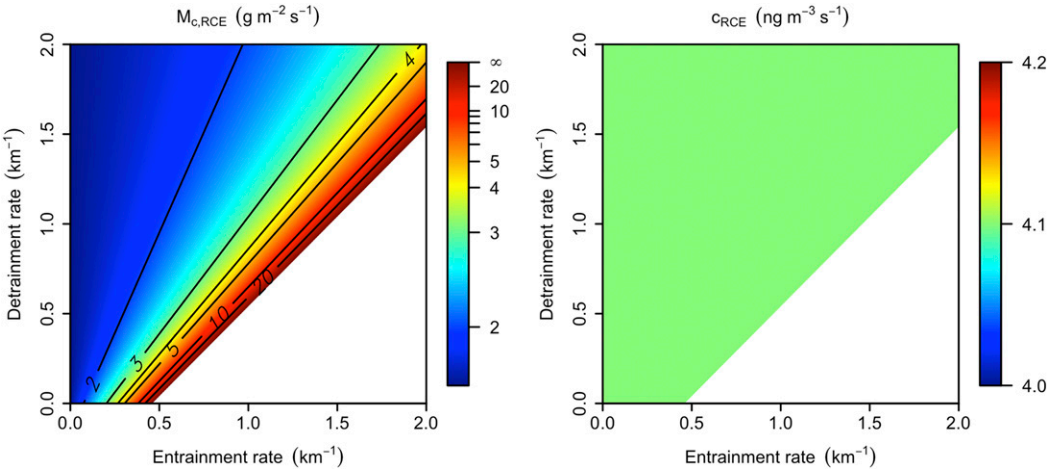

FIG. 1. For RCE (i.e., $\tilde{M} = 0$) at $T = 300\,\mathrm{K}$ and $p = 100\,\mathrm{kPa}$ with $Q = 0.01\,\mathrm{W\,m^{-3}}$, (left) cloud mass flux and (right) condensation rate, both as functions of the fractional rates of entrainment and detrainment. The condensation rate is plotted here to emphasize that it is independent of the entrainment and detrainment rates; in RCE, it must balance the radiative cooling.

RCE. We can also define the lapse rate Γ, the inverse of the water-vapor-scale height γ, and the relative humidity RH as $\Gamma = -\partial T/\partial z$, $\gamma = -\partial \log(q_v^*)/\partial z$, and $\mathrm{RH} = q_v/q_v^*$, respectively. With these definitions, and assuming that RH varies over distances that are large compared to $1/\gamma$, we can then find analytic solutions for RH, γ, Γ, r, $\tilde{c}$, $\tilde{M}_c$, and $\tilde{M}_e$ as explicit functions of $\tilde{M}$ that do not depend on the radiative cooling rate Q. These RCAE solutions are given in Eqs. (A37)–(A43) in the appendix.

3. Behavior of the solutions

The solutions are plotted in Fig. 2 for $T = 300\,\mathrm{K}$, $p = 100\,\mathrm{kPa}$, and $\varepsilon = \delta = 0.5\,\mathrm{km^{-1}}$. Because Q has dropped out the solutions, the variables plotted in Fig. 2 are functions only of $\tilde{M}$. To show the limiting behavior of the solutions, the abscissa ranges over -10 to 10. Black circles mark the RCE values at $\tilde{M} = 0$.

The limiting values of RH are

$$\mathrm{RH} = \begin{cases} 1 & \tilde{M} = \infty \\ \dfrac{\varepsilon - \varepsilon_0}{\varepsilon} & \tilde{M} = -\infty \end{cases}, \tag{14}$$

where

$$\varepsilon_0 \equiv \frac{g}{c_p T}\left(\frac{L}{R_v T} - \frac{c_p}{R_a}\right). \tag{15}$$

In the limit of rapid ascent, we see that the column becomes saturated (RH = 1). In RCE (i.e., $\tilde{M} = 0$), the relative humidity takes an intermediate value derived previously by Romps (2014). In the limit of rapid descent, the relative humidity asymptotes not to zero but to a finite value that is nonnegative so long as $\varepsilon \geq \varepsilon_0$. For $p = 100\,\mathrm{kPa}$ and $T = 300\,\mathrm{K}$, $\varepsilon_0 = 0.46\,\mathrm{km^{-1}}$; for ε greater than this value (e.g., the value of $0.5\,\mathrm{km^{-1}}$ used in Fig. 2), the solution remains physical for all values of $\tilde{M}$.

The limiting values of the lapse rate are

$$\Gamma = \begin{cases} \dfrac{g\left(1 + \dfrac{q_v^* L}{R_a T}\right)}{c_p + \dfrac{q_v^* L^2}{R_v T^2}} & \tilde{M} = \infty \\ \dfrac{g}{c_p} & \tilde{M} = -\infty \end{cases}. \tag{16}$$

In the limit of rapid ascent, the lapse rate equals the moist adiabat. In RCE, the lapse rate takes an intermediate value derived by Romps (2014). In the limit of rapid descent, the lapse rate asymptotes to a dry adiabat.

The limiting values of the condensation rate are

$$\tilde{c} = \begin{cases} \infty & \tilde{M} = \infty \\ \dfrac{\varepsilon - \varepsilon_0}{\delta} & \tilde{M} = -\infty \end{cases}. \tag{17}$$

In the limit of rapid ascent, the condensation rate tends to infinity. In RCE, $\tilde{c} = 1$. In the limit of rapid descent, the condensation rate asymptotes not to zero but to a finite value that is nonnegative so long as $\varepsilon \geq \varepsilon_0$. Recalling that the lapse rate equals the dry adiabat in the rapid-descent limit, it may sound odd that there could be nonzero condensation in that limit. This apparent contradiction (precipitating dry-adiabatic clouds) is resolved by noting that the cloud mass flux tends to infinity in this limit. Therefore, the condensation rate per unit of cloud mass flux can go to zero while maintaining a finite domain-wide condensation rate.

Figure 3 plots the solutions for five different values of ε (0.1, 0.2, 0.5, 1, and $2\,\mathrm{km^{-1}}$) with $\delta = \varepsilon$ in all cases. The green curves are the same as in Fig. 2. Note that the abscissa in Fig. 3 ranges from -2 to 2 instead of -10 to 10. In the sections that follow, let us refer to these solutions as the zero-buoyancy solutions. This terminology emphasizes the solutions' defining characteristic:

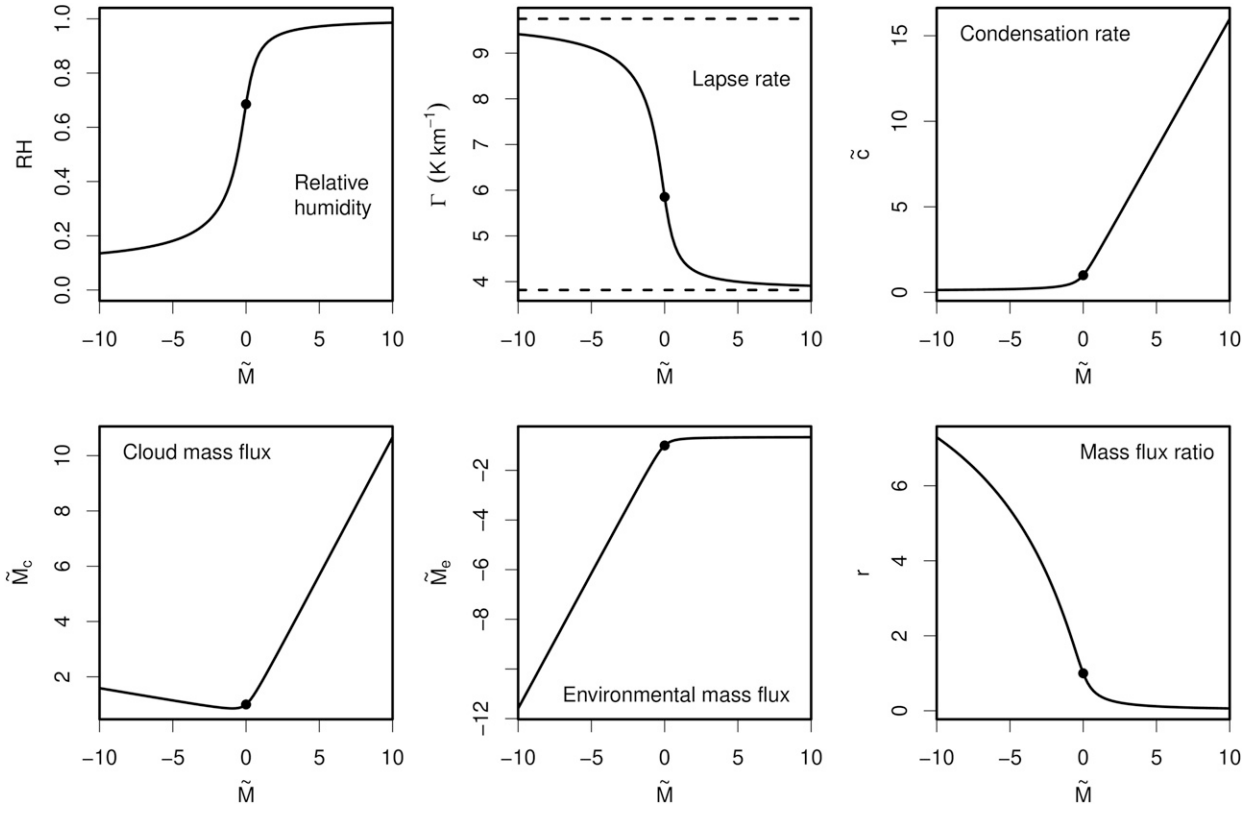

FIG. 2. Solutions from Eqs. (A37)–(A43) with $p = 100$ kPa, $T = 300$ K, and $\varepsilon = \delta = 0.5\ \mathrm{km}^{-1}$. Circles denote values in RCE, i.e., at $\tilde{M} = 0$. Dashed lines in the plot of lapse rate mark the moist and dry adiabats.

given M and Q, the solutions give the state of the atmosphere that would be consistent with zero-buoyancy convection.

4. Do the solutions explain tropical variability?

A series of papers (Singh and O'Gorman 2013; Singh et al. 2017, 2019) claimed to show that the zero-buoyancy solutions are useful for understanding the covariation of RH, CAPE, and precipitation in the tropics. Sections 4a and 4b will re-examine the proffered evidence. Section 4c will explain that the zero-buoyancy solutions fail as a model for tropical variability because they neglect the gravity waves that enforce the tropic's weak temperature gradient (WTG).

a. Variability of CAPE

Singh and O'Gorman (2013) looked at soundings from the tropical Pacific warm pool (their Fig. 3) and found that high RH and high CAPE do not coexist. The proposed explanation was based on the zero-buoyancy solutions: high RH causes a low lapse rate, i.e., high stability and, therefore, low CAPE. But this explanation would produce spatial variations in the lapse rate that are incompatible with WTG. Very roughly, using a gravitational acceleration of $10\ \mathrm{m\,s}^{-2}$, a mean tropospheric temperature of 250 K, and a tropospheric depth of 10^4 m, each 1 K of virtual temperature anomaly adds ~400 J of additional CAPE ($10 \times 10^4/250 = 400$). Singh and O'Gorman (2013) interpreted their Fig. 3 as showing that variations in RH cause variations in CAPE ranging from 0 to 1500 J. That would imply horizontal variations in tropospheric temperature of ~4 K, which is incompatible with the observed variations of ~1 K (see section 4c). Instead, high RH and high CAPE are rarely found together because such a state would be highly unstable. If the high CAPE were caused by high boundary layer entropy, then the entraining convection would thrive in the high-RH troposphere and would reduce RH, CAPE, or both. If the high CAPE were caused by an especially cold troposphere, then gravity waves would act to heat the column, thereby reducing CAPE and enforcing WTG.

Singh et al. (2017) looked at all available soundings from 36°S to 36°N and found that conditionally averaged CAPE roughly doubles as the lower-tropospheric saturation deficit grows from zero to its median value (their Fig. 3 and Fig. S5). Again, the explanation for this was based on the zero-buoyancy solutions: a higher saturation deficit causes a higher lapse rate and, therefore, higher CAPE. Figure 4a in this paper plots the conditionally averaged CAPE (red squares) as a function of saturation deficit using the same data and, to the extent replicable, the same methods. As in Singh et al. (2017), CAPE roughly doubles as the saturation deficit increases from zero to its median value. Note, however, that this does not show CAPE varying with saturation deficit *with all else equal*. By looking at 36°S to 36°N, this has included soundings from places that are

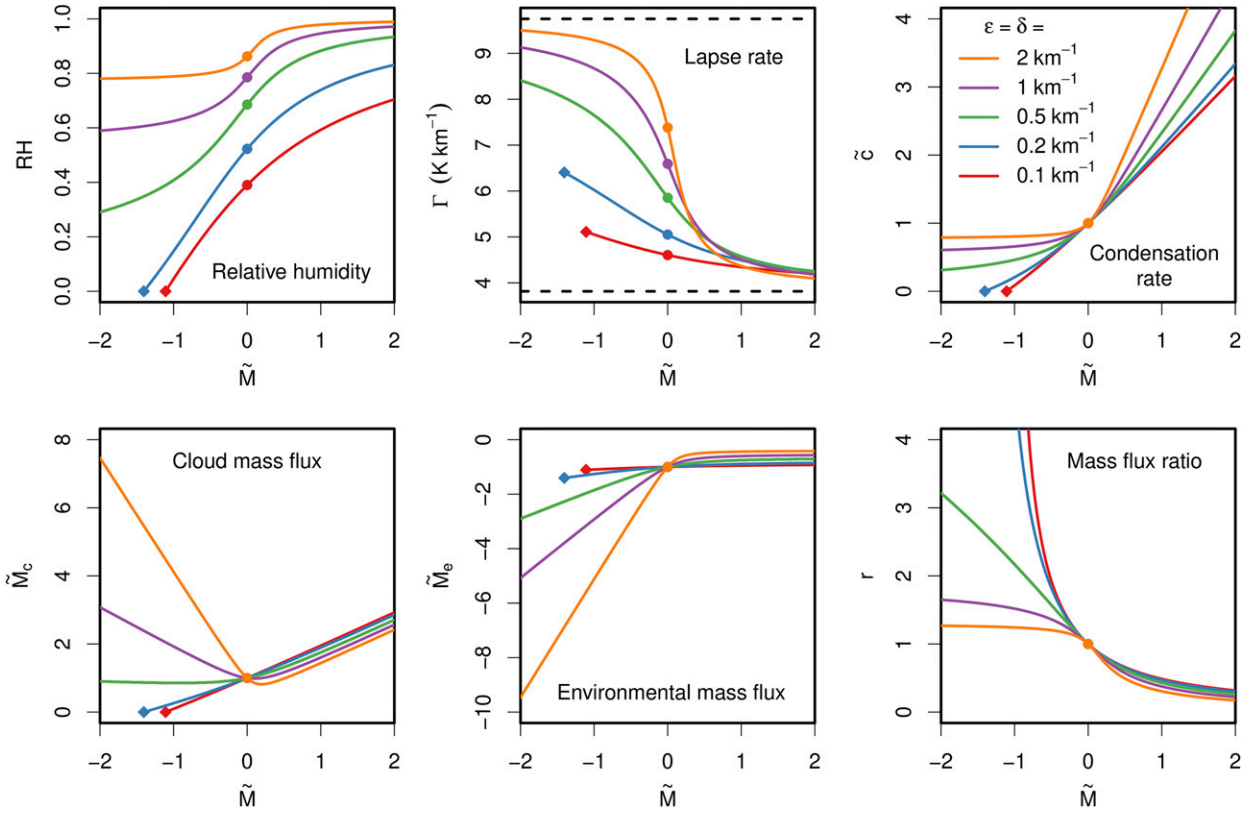

FIG. 3. As in Fig. 2, but with $\varepsilon = \delta$ ranging from 0.1 to 2 km^{-1}. Diamonds mark the RH = 0 solutions in cases where $\varepsilon < \varepsilon_0$.

in no way tropical (e.g., Oklahoma City and Gwangju, South Korea, whose average lows are below freezing in winter). Indeed, if we plot conditionally averaged temperature as a function of saturation deficit (blue plusses), we see that the low CAPE at low saturation deficit is caused, in large part, by the inclusion of cold nontropical soundings. Instead, if we restrict to 15°S to 15°N, the conditionally averaged surface air temperature varies over less than 2 K and the conditionally averaged CAPE behaves as shown in the red squares of Fig. 4b.

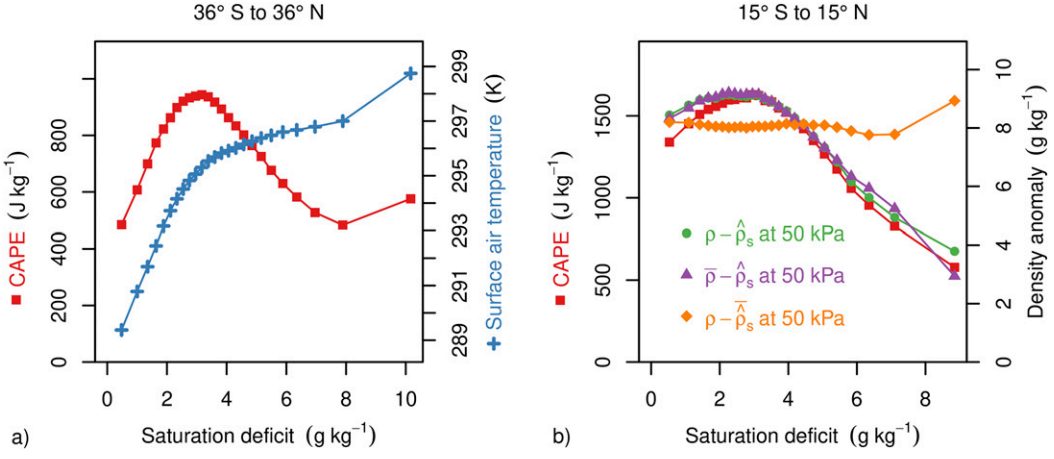

FIG. 4. (a) For soundings between 36°S and 36°N, conditionally averaged CAPE (red squares) and surface air temperature (blue plus signs) as functions of the lower-tropospheric saturation deficit. (b) For soundings between 15°S and 15°N, conditionally averaged CAPE (red squares), lifted-parcel density anomaly $\rho - \hat{\rho}_s$ at 50 kPa (green circles), $\overline{\rho} - \hat{\rho}_s$ at 50 kPa (purple triangles), and $\rho - \overline{\hat{\rho}}_s$ at 50 kPa (orange diamonds).

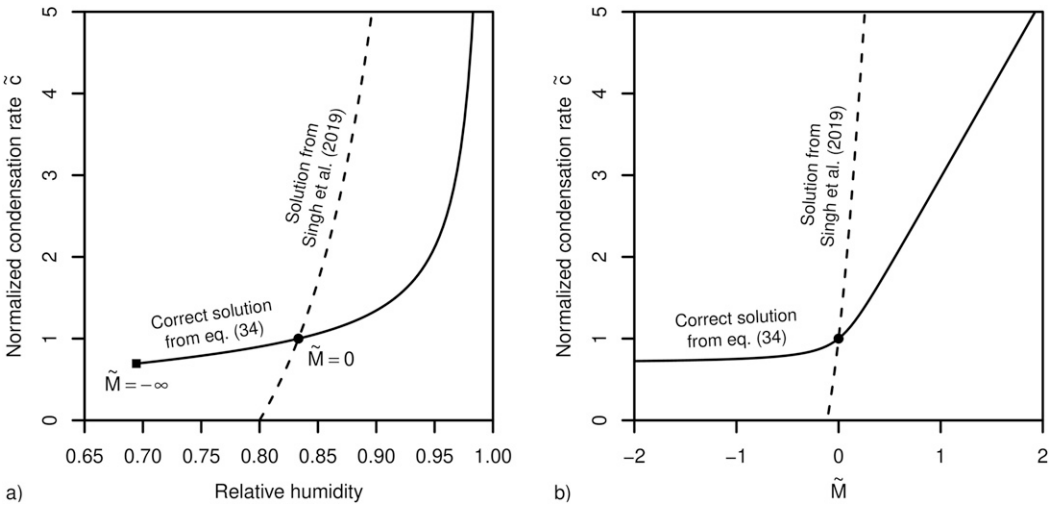

FIG. 5. (a) Normalized condensation rate $\tilde{c}$ plotted against relative humidity for the correct solution given by Eq. (18) (solid) and Eq. (15) (dashed) of Singh et al. (2019). For both curves, $p = 100$ kPa, $T = 300$ K, and $\varepsilon = \delta = 1.5\,\mathrm{km}^{-1}$ to match the RCE relative humidity of 83% as in Fig. 1 of Singh et al. (2019). The circle marks the RCE solution and the square marks the solution with infinite mean descent. (b) As in (a), but with $\tilde{c}$ plotted against $\tilde{M}$.

What causes the unimodal shape of CAPE in Fig. 4b? To find out, let us denote the density of a lifted surface air parcel as $\hat{\rho}_s$, which is a function of the isobar to which it is lifted, and let us write the environmental density as ρ, also a function of isobar. Their difference $(\rho - \hat{\rho}_s)$ evaluated at 50 kPa is plotted in green circles, and we see that this density anomaly is an excellent proxy for CAPE. Using a bar to denote an unconditional average over all soundings, we can figure out what causes the variation in CAPE by also plotting $\overline{\rho} - \hat{\rho}_s$ (purple triangles) and $\rho - \overline{\hat{\rho}}_s$ (orange diamonds). These show that the variation in CAPE is entirely explained by variations in surface air entropy, with virtually zero contribution from variations in free-tropospheric density or, equivalently, free-tropospheric virtual temperature. Contrary to the prediction of the zero-buoyancy solutions, the local saturation deficit does not control the local free-tropospheric temperature.

b. *Variability of precipitation*

Singh et al. (2019) found that the precipitation rate (i.e., condensation rate) goes to zero at a critical relative humidity $\mathrm{RH}_{\mathrm{min}}$ in their zero-buoyancy solutions [see their Eq. (15)]. Noting that precipitation relates nonlinearly with RH in the tropics, this was cited as evidence for the usefulness of the zero-buoyancy solutions in understanding the covariation of tropical RH and precipitation. As mentioned earlier, however, Singh et al. (2019) made a mathematical error in their derivation. One clue that something is awry with their solutions is that their sensitivity to relative humidity is extreme. By Eq. (15) of Singh et al. (2019), the difference between their minimum relative humidity ($\mathrm{RH}_{\mathrm{min}}$, at which precipitation turns on) and the RCE relative humidity ($\mathrm{RH}_{\mathrm{RCE}}$, at $\tilde{M} = 0$) is $(\mathrm{RH}_{\mathrm{RCE}} - 1)^2/\mathrm{RH}_{\mathrm{RCE}}$. For $\mathrm{RH}_{\mathrm{RCE}} = 0.83$ as in Singh et al. (2019), this implies that precipitation shuts off if the relative humidity drops from its RCE value by only 3%, implying that RCE sits on the knife's edge, just barely able to precipitate.

This behavior, however, is spurious: with the correct solutions derived here, we can see that there is no such behavior. The general solution for $\tilde{c}$, given by Eqs. (A40) and (A41), tells us that

$$\tilde{c} = \frac{(A - B\mathrm{RH})\mathrm{RH}}{\delta(1 - \mathrm{RH})}, \tag{18}$$

where A and B are defined in Eqs. (A28) and (A29) in the appendix. Since $A > B > 0$, this tells us that the condensation rate is positive for all positive values of RH. This relationship between condensation and relative humidity is plotted as the solid curve in Fig. 5a using $\varepsilon = \delta = 1.5\,\mathrm{km}^{-1}$ to match the RCE RH of 0.83 in Fig. 1 of Singh et al. (2019). Around RCE, the solution of Singh et al. (2019) gives a precipitation rate that varies with relative humidity more than 10 times too rapidly. And, in the correct solution, there is no special RH at which the condensation rate suddenly turns on.

It is tempting to look at the correct solution in Fig. 5a and conclude that the convection shuts off at a relative humidity of 0.69, but that would be wrong. In the zero-buoyancy solutions, relative humidity is not an independent variable: instead, it is set internally by the interplay between convection and its environment. The external control is the mean ascent rate $\tilde{M}$, and both the relative humidity and the condensation rate asymptotically approach finite values as $\tilde{M}$ goes to negative infinity. Thus, while it is fine to make plots like Fig. 5a, it must be understood that relative humidity is not "controlling" the condensation rate, the lapse rate, or CAPE any more than the reverse is true. Figure 5b plots the condensation rate as a function of the independent variable $\tilde{M}$, which shows that the correct solution continues to have $\tilde{c} \geq 0.69$ no matter what the value of $\tilde{M}$ is. In other words, as a model for tropical variability,

these solutions would predict that everywhere in the tropics precipitates at a rate at least 69% as high as RCE. The real tropics are not like this at all.

c. *Why the solutions fail as a model of variability*

We have seen that the zero-buoyancy solutions fail to explain the tropical covariation of RH, CAPE, and precipitation. The fundamental reason for this failure is that these solutions are for an atmosphere in a box decoupled from its surroundings: that atmosphere in a box does not feel or adjust to the lapse rate of neighboring patches of atmosphere, thereby violating the tropical WTG.

In fact, the bulk-plume solutions violate WTG in a rather spectacular fashion. From the solution for Γ in Eq. (A39), we learn that the lapse rate Γ is linear in RH. In particular,

$$\frac{\partial \Gamma}{\partial \mathrm{RH}} = -\frac{q_v^* L \varepsilon}{c_p + \dfrac{q_v^* L^2}{R_v T^2}}. \tag{19}$$

With the same parameters used for Fig. 2 ($p = 100\,\mathrm{kPa}$, $T = 300\,\mathrm{K}$, $\varepsilon = \delta = 0.5\,\mathrm{km}^{-1}$), this gives $-6.5\,\mathrm{K\,km}^{-1}$, which means, e.g., that a change in RH by 50% (e.g., from 50% to 100%) reduces the lapse rate by $3.3\,\mathrm{K\,km}^{-1}$. Integrated over the scale height of water vapor $1/\gamma$ ($\approx 4.4\,\mathrm{km}$), this would lead to a temperature difference of $\approx 14\,\mathrm{K}$ at a height of 5 km between a patch of saturated atmosphere and a patch of atmosphere with a relative humidity of 50%. In the tropics, such large temperature variations are unrealizable due to efficient gravity waves, which maintain a weak temperature gradient. Using the Integrated Global Radiosonde Archive (IGRA) database (Durre et al. 2006) and restricting to soundings in the deep tropics (15°S to 15°N), where planetary rotation is small, the interquartile range of temperature at 5 km is only 1.6 K. (No effort has been made here to detrend the sounding data for the effect of global warming, so this interquartile range, impressively small already, is biased high.) Repeating this analysis with radiosonde data from the U.S. Department of Energy (DOE) Atmospheric Radiation Measurement (ARM) tropical western Pacific (TWP; Mather et al. 1998) sites in Darwin, Manus, and Nauru from 2001 to 2015, the interquartile ranges for the temperature and virtual temperature at 5 km are found to be 1.4 and 1.3 K, respectively, confirming the near absence of temperature variation.

Not only is WTG obeyed in the tropics, but the small temperature variations have no meaningful correlation with the relative humidity, as we saw in Fig. 4b. To illustrate this in another way, Fig. 6 shows the virtual temperature at 5 km in the deep tropics plotted at 10 percentiles (5th through 95th) of the relative humidity of the lower troposphere (defined as the mean of the relative humidities at the 85-, 70-, and 50-kPa levels, weighted by their saturation specific humidity). At each relative humidity, the median and interquartile range of the 5-km virtual temperature is plotted. Note that the mid-tropospheric virtual temperature does not vary with lower-tropospheric humidity.

Also shown in Fig. 6 are the predictions for those temperatures if the 5-km temperature were controlled by local convection, as is assumed in the zero-buoyancy solutions. For the purposes of illustration, we will take the lapse rate predicted by Eq. (A39) (using the mean observed properties at the standard pressure level of 70 kPa), multiply that lapse rate by 5 km, and subtract that from 300 K to predict the temperature at a height of 5 km. As mentioned earlier, the observed surface air temperature varies by less than 2 K when conditionally averaged on saturation deficit, so measuring the temperature at 5 km is tantamount to measuring the integrated lapse rate up to that height. The results are plotted in Fig. 6 for three different entrainment rates, with δ set to ε in each case. For all of the model solutions, the slope of $T(5\,\mathrm{km})$ versus RH is entirely inconsistent with the observations.

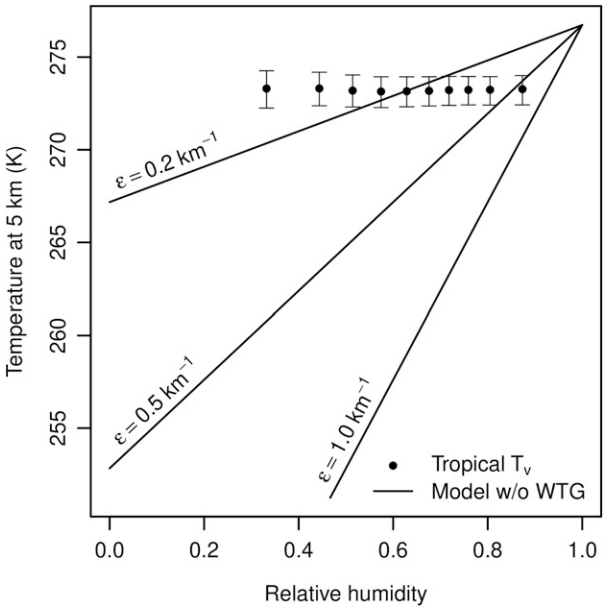

FIG. 6. A comparison of the dependence of the 5-km temperature on the lower-tropospheric humidity as (lines) predicted by the zero-buoyancy bulk-plume model for three different fractional entrainment rates with $\delta = \varepsilon$ and (circles) observed in the deep tropics. Circles give the median virtual temperature at 5 km at each of 10 percentiles (5th through 95th) of lower-tropospheric relative humidity. Whiskers show the interquartile range. Lines show the bulk-plume prediction from Eq. (A39).

What we can infer from Fig. 6 is that the tropics have a lapse rate that is everywhere consistent with an ascending zero-buoyancy solution with a relative humidity of ~0.8 and an entrainment rate of $\sim 0.5\,\mathrm{km}^{-1}$. This roughly matches what we know: tropical precipitation occurs mostly in regions with lower-tropospheric relative humidity in the range of 0.7–0.8 (Bretherton et al. 2004) and large-eddy simulations find that the mean lower-tropospheric bulk-plume entrainment rate for tropical deep convection is in the ballpark of $0.5\,\mathrm{km}^{-1}$ (e.g., Romps 2010).

To reiterate, the zero-buoyancy bulk-plume solutions fail as a model of the covariation of tropical RH, CAPE, and precipitation because they assume that the lapse rate is set locally. In reality, the lapse rate of a patch of tropical atmosphere is predominantly controlled by an appropriate average

of moist convection throughout the tropics, not by the convection (if any) that is local to the patch.[2] The value of the zero-buoyancy solutions is not that they explain variance in the tropics, but that they can tell us about the mean RH, CAPE, and precipitation rate of the deeply convecting regions and the mean lapse rate that they impart to the whole tropics.

5. The aggregated state

According to this interpretation, the deep tropics provides only a single realization of a zero-buoyancy solution. To provide additional checks of the theory, we can turn to numerical simulations. Here, we will see if the theory can predict the properties of the convectively aggregated state.

To build a toy model for the aggregated state, we can stitch together a zero-buoyancy ascending solution with a nonconvecting dry patch. A steady-state descending column does not have deep convection because its lapse rate is set by ascending convecting regions elsewhere, and that lapse rate is smaller than is required for a zero-buoyancy solution with $M < 0$. For such dry patches, we can set Γ to the value from the convecting regions. For the mean relative humidity of the dry patch, we will simply approximate it as zero as would be appropriate for a circulation that converges air into the dry patch in the upper troposphere; the results below can be generalized easily to a dry-patch relative humidity that is some nonzero fraction of the moist patch's relative humidity. The environment descends in this nonconvecting region at the same speed as in the convecting region, as given by Eq. (7).

If the convecting region occupies a fraction f of the domain, then mass conservation requires

$$(1-f)M_e + fM = 0. \tag{20}$$

Rearranging, we find that

$$f = -\frac{M_e}{M_c}. \tag{21}$$

From Eq. (A41) in the appendix, $-M_e/M_c = \tilde{c}$, so

$$\tilde{c} = \frac{1}{f}. \tag{22}$$

Since there is no condensation in the dry patch, the normalized domain-mean condensation rate $\tilde{c}_{\rm ave}$ is equal to $f\tilde{c}$, which, combined with (22), gives

$$\tilde{c}_{\rm ave} = 1. \tag{23}$$

Equations (22) and (23) tell us that the radiative cooling throughout the domain is balanced by the latent heating in the convecting portion of the domain.

[2] Note the key word "predominantly." Of course, local convection does have some influence on the local temperature, and the resulting small temperature variations are essential to establishing large-scale circulations. But gravity waves are so efficient that circulations can be established with only small deviations from the tropical mean temperature profile.

Next, combining (21) with (A40) in the appendix, the relative humidity in the convecting region is found to be

$$\mathrm{RH} = \frac{\delta + fA - \sqrt{(\delta + fA)^2 - 4fB\delta}}{2fB}, \tag{24}$$

where A and B are given by Eqs. (A28) and (A29) in the appendix. Using our approximation of $q_v = 0$ in the nonconvecting region, the domain-mean relative humidity is simply

$$\mathrm{RH}_{\rm ave} = f\,\mathrm{RH}. \tag{25}$$

Finally, to get an expression for Γ in terms of f, we can combine (24) with (A39) in the appendix to get

$$\Gamma = \frac{R_v T^2}{L}\left(\frac{-\delta + fA + \sqrt{(\delta + fA)^2 - 4fB\delta}}{2f} + \frac{g}{R_a T}\right). \tag{26}$$

Figure 7 plots RH and $\mathrm{RH}_{\rm ave}$ (left panel), the lapse rate (middle panel), and the condensation rates (right panel) as functions of f for five different entrainment rates. The RCE case corresponds to $f = 1$, where convection is uniformly distributed through the entire domain. As f decreases, the convection is aggregated into a fraction f of the domain.

As the convection aggregates, the relative humidity in the convecting patch increases while the domain-mean relative humidity decreases, a behavior that is found in numerical simulations (Held et al. 1993; Bretherton et al. 2005; Wing et al. 2017). We can understand this behavior as follows: RH in the convecting patch goes to one as f goes to zero because the convection is increasingly concentrated in a smaller area, causing detrainment moistening to overwhelm subsidence drying there. While the convecting patch approaches saturation as it contracts, the domain-mean relative humidity is given by fRH, which, in the limit of small f, simply equals f.

We also see that the lapse rate decreases as the atmosphere aggregates; this, too, is found in numerical simulations of convective aggregation (Held et al. 1993; Wing and Cronin 2016; Wing et al. 2017; Becker et al. 2018). We can understand this by noting that RH approaches one as the convecting patch contracts to zero size, for the reason just noted. As RH approaches unity, the effect of entrainment vanishes, so the lapse rate asymptotically approaches a moist adiabat.

Finally, as the convection aggregates, the fixed rate of domain-mean condensation occurs in a smaller area, causing $\tilde{c}$ to increase. This is a robust feature of every numerical simulation of convective aggregation, reflected in the very high precipitation rate in the convecting patch. In this toy model, Q is held fixed, so the domain-mean condensation rate does not change with aggregation. In models with interactive radiation, the redistribution of water vapor and clouds can alter the net radiative cooling of the troposphere, leading to small fractional changes in the domain-mean precipitation rate [e.g., the $\lesssim$10% decrease seen by Held et al. (1993)].

6. Summary

Using a zero-buoyancy bulk-plume model of a convecting atmosphere, analytic solutions have been derived for the

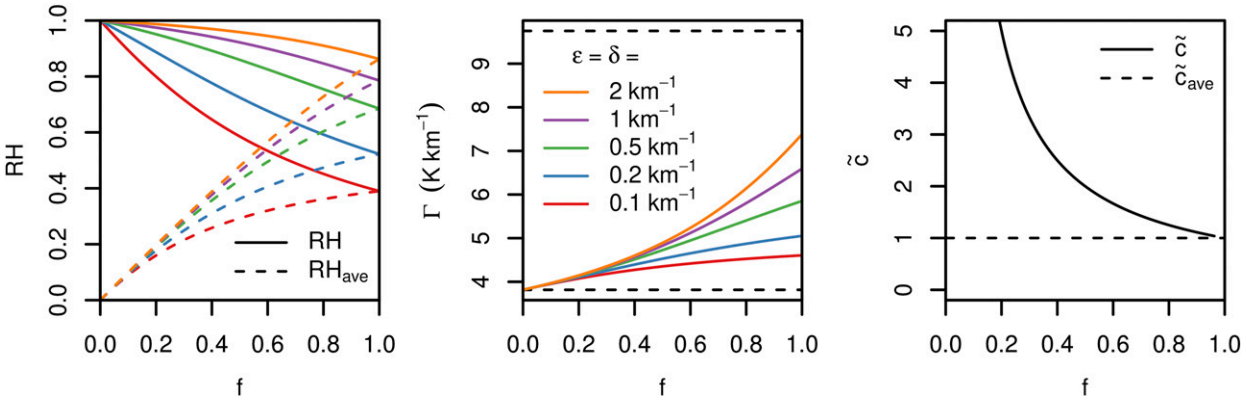

FIG. 7. (left) As a function of the fraction f of the domain that is convecting, RH in the convecting fraction of the domain (solid) and the domain-mean RH plotted for five different fractional entrainment rates (dashed). (center) The lapse rate as a function of f for the five different entrainment rates. The dashed lines mark the dry and moist adiabats. (right) The normalized condensation rate in the convecting region ($\tilde{c}$; solid) and averaged throughout the domain ($\tilde{c}_{\text{ave}}$; dashed). The curves are colored black here because the condensation rates, expressed as functions of f, are independent of the entrainment rate.

relative humidity, lapse rate, condensation rate, cloud mass flux, and environmental mass flux as functions of the pressure, temperature, fractional rates of entrainment and detrainment, radiative cooling, and the net mass flux (or, instead of the net mass flux, the fraction of the domain that is deeply convecting). This extends the solutions in Romps (2014) to nonzero net vertical mass flux (see Fig. 3). As in Romps (2014), these solutions can be integrated numerically in the vertical to produce full atmospheric profiles, although that has not been done here.

Several papers (Singh and O'Gorman 2013; Singh et al. 2017, 2019) have argued that the zero-buoyancy solutions can explain much of the covariation of RH, CAPE, and precipitation in the tropics. As argued in section 4, the evidence does not support this claim and, further, the idea is incompatible with the tropics' weak temperature gradient (WTG; see Fig. 6). Instead, it is appropriate to use an ascending zero-buoyancy solution to describe the mean properties (RH, CAPE, lapse rate, and precipitation rate) of tropical regions that are deeply convecting and, thanks to efficient gravity waves, the thermal structure of the free troposphere throughout the tropics.

In section 5, we constructed an aggregated state by stitching together an ascending and convecting patch of atmosphere to a descending and nonconvecting patch of atmosphere using the WTG approximation. As the convection aggregates, the relative humidity and precipitation rate increase in the ascending region, the domain-mean relative humidity decreases, the domain-mean precipitation stays the same (assuming a fixed radiative cooling rate), and the lapse rate decreases (see Fig. 7). These behaviors match what has been found in cloud-resolving simulations of convective aggregation, bolstering the notion that these zero-buoyancy solutions are an appropriate toy model for the mean properties of convecting regions.

Acknowledgments. This work was supported by the U.S. Department of Energy's (DOE) Atmospheric System Research (ASR), an Office of Science, Office of Biological and Environmental Research program; Lawrence Berkeley National Laboratory is operated for the DOE by the University of California under Contract DE-AC02-05CH11231. Data were obtained from the Atmospheric Radiation Measurement (ARM) user facility, a U.S. DOE Office of Science user facility managed by the Biological and Environmental Research Program. Integrated Global Radiosonde Archive (IGRA) version 2 data were provided by the National Oceanic and Atmospheric Administration (NOAA) National Centers for Environmental Information (NCEI). The author wishes to extend particular thanks to Martin Singh for his thoughtful and helpful feedback on this manuscript.

APPENDIX

Zero-Buoyancy Solutions

To solve Eqs. (1)–(6), we will first derive expressions for the condensation rate and the relative humidity. With the aid of (1) and (2), we can write (3)–(6) as

$$M_c \frac{\partial}{\partial z} q_v^* = e(q_v - q_v^*) - c, \tag{A1}$$

$$M_e \frac{\partial}{\partial z} q_v = d(q_v^* - q_v), \tag{A2}$$

$$M_c \frac{\partial}{\partial z} h^* = e(h - h^*), \tag{A3}$$

$$M_e \frac{\partial}{\partial z} h = d(h^* - h) + Q. \tag{A4}$$

Following Romps (2014), these can be simplified by introducing γ defined as $\gamma \equiv -\partial \log(q_v^*)/\partial z$, the relative humidity defined as $\text{RH} \equiv q_v/q_v^*$, and the fractional entrainment and detrainment rates defined as $\varepsilon \equiv e/M_c$ and $\delta \equiv d/M_c$, respectively. Written in terms of these variables, Eq. (A1) becomes an expression for the condensation rate,

$$c = [\gamma - \varepsilon(1 - \text{RH})] M_c q_v^*. \tag{A5}$$

Since all condensates are assumed to fall out of the atmosphere immediately upon formation, c represents the generation of precipitation. Next, using the fact that $q_v = \mathrm{RH}q_v^*$, applying the definitions of γ, δ, and $r \equiv -M_e/M_c$, and ignoring the small fractional vertical variations in RH, Eq. (A2) can be rewritten as an expression for RH,

$$\mathrm{RH} = \frac{\delta}{\delta + r\gamma}. \tag{A6}$$

As noted by Singh et al. (2019), this expression for RH generalizes the expression obtained by Romps (2014) to non-RCE cases (i.e., $r \neq 1$). But Eq. (A5) for the condensation rate and Eq. (A6) for the relative humidity both depend on the unknown γ, so our derivation is not yet complete.

As shown by Romps (2014), γ (defined as $-\partial \log q_v^*/\partial z$) is related to the lapse rate Γ (defined as $-\partial T/\partial z$) by

$$\gamma = \frac{L\Gamma}{R_v T^2} - \frac{g}{R_a T}, \tag{A7}$$

where R_v and R_a are the specific gas constants of water vapor and dry air, respectively. Next, consider the definitional equation for h^*, which is $h^* = c_p T + Lq_v^* + gz$. Taking $\partial/\partial z$ of this definitional equation and then using Eq. (A7) to rewrite γ in terms of Γ, we get

$$\frac{\partial h^*}{\partial z} = g\left(1 + \frac{q_v^* L}{R_a T}\right) - \Gamma\left(c_p + \frac{q_v^* L^2}{R_v T^2}\right). \tag{A8}$$

Another expression for $\partial h^*/\partial z$ can be obtained by dividing (A3) by M_c and using the fact that $h - h^* = L(q_v - q_v^*) = L(\mathrm{RH} - 1)q_v^*$. This gives

$$\frac{\partial h^*}{\partial z} = \varepsilon L(\mathrm{RH} - 1)q_v^*. \tag{A9}$$

Equating the right-hand sides of Eqs. (A8) and (A9) produces

$$\Gamma = \frac{g\left(1 + \frac{q_v^* L}{R_a T}\right) + q_v^* L\varepsilon(1 - \mathrm{RH})}{c_p + \frac{q_v^* L^2}{R_v T^2}}. \tag{A10}$$

This expression for Γ is valid in the zero-buoyancy approximation for RCE and non-RCE atmospheres alike. Note that it is a linear function of RH. Using (A7), we can obtain from this a similar expression for γ:

$$\gamma = A - B\mathrm{RH}, \tag{A11}$$

where A and B are constants given below.

Our penultimate task is to find a relationship between Q, r, and c. Multiplying (A1) by r and adding it to (A2), and likewise multiplying (A3) by r and adding it to (A4), we get

$$M_e \frac{\partial}{\partial z}(q_v - q_v^*) = (d - re)(q_v^* - q_v) - rc, \tag{A12}$$

$$M_e \frac{\partial}{\partial z}(h - h^*) = (d - re)(h^* - h) + Q. \tag{A13}$$

Multiplying (A12) by L and replacing $h - h^*$ with $L(q_v - q_v^*)$ in (A13), we get

$$LM_e \frac{\partial}{\partial z}(q_v - q_v^*) = L(d - re)(q_v^* - q_v) - Lrc, \tag{A14}$$

$$LM_e \frac{\partial}{\partial z}(q_v - q_v^*) = L(d - re)(q_v^* - q_v) + Q. \tag{A15}$$

Subtracting (A14) from (A15), we are left with

$$c = -\frac{Q}{rL}. \tag{A16}$$

For a given Q, c is inversely proportional to r.

We are now ready to solve the system of Eqs. (1)–(6). Using (A11) in (A6) and solving for r, we get

$$r = \frac{\delta/\mathrm{RH} - \delta}{A - B\mathrm{RH}}. \tag{A17}$$

Taking one minus (A17) and dividing by (A17), we get

$$\frac{1 - r}{r} = \frac{-B\mathrm{RH}^2 + (A + \delta)\mathrm{RH} - \delta}{\delta(1 - \mathrm{RH})}. \tag{A18}$$

Next, we can use (A11) and $M_c = M/(1 - r)$ to write (A5) as

$$c = [A - B\mathrm{RH} - \varepsilon(1 - \mathrm{RH})]\frac{M}{1 - r}q_v^*. \tag{A19}$$

Using (A16) to replace c in (A19) and multiplying both sides by $1 - r$, we get

$$\frac{1 - r}{r} = -\frac{Q}{MLq_v^*}[A - B\mathrm{RH} - \varepsilon(1 - \mathrm{RH})]. \tag{A20}$$

Equating the right-hand sides of (A18) and (A20) gives a quadratic equation for RH in terms of constants (T, p, ε, δ), thermodynamic functions of those constants (q_v^* and L), and control parameters (Q and M).

Altogether, the solution for the state of the atmosphere is

$$\mathrm{RH} = \frac{-b_2 - \sqrt{b_2^2 - 4b_1 b_3}}{2b_1}, \tag{A21}$$

$$\gamma = A - B\mathrm{RH}, \tag{A22}$$

$$\Gamma = \frac{R_v T^2}{L}\left(A - B\mathrm{RH} + \frac{g}{R_a T}\right), \tag{A23}$$

$$r = \frac{\delta(1 - \mathrm{RH})}{(A - B\mathrm{RH})\mathrm{RH}}, \tag{A24}$$

$$c = -\frac{Q}{Lr}, \tag{A25}$$

$$M_c = \frac{c/q_v^*}{\gamma - \varepsilon(1 - \mathrm{RH})}, \tag{A26}$$

$$M_e = M - M_c, \tag{A27}$$

where the constants A, B, b_1, b_2, and b_3 are defined as

$$A = \frac{L}{R_v T^2}\frac{g\left(1+\frac{q_v^* L}{R_a T}\right)+q_v^* L\varepsilon}{c_p+\frac{q_v^* L^2}{R_v T^2}}-\frac{g}{R_a T}, \tag{A28}$$

$$B = \frac{L}{R_v T^2}\frac{q_v^* L\varepsilon}{c_p+\frac{q_v^* L^2}{R_v T^2}}, \tag{A29}$$

$$b_1 = \frac{B}{\delta}+M(\varepsilon-B)\frac{Lq_v^*}{Q}, \tag{A30}$$

$$b_2 = -\frac{A+\delta}{\delta}+M(A+B-2\varepsilon)\frac{Lq_v^*}{Q}, \tag{A31}$$

$$b_3 = 1+M(\varepsilon-A)\frac{Lq_v^*}{Q}. \tag{A32}$$

We can simplify these solutions further by removing any explicit dependence on Q. In RCE, $M = 0$ and the expression for RH simplifies to

$$\mathrm{RH}_{\mathrm{RCE}} = \frac{A+\delta-\sqrt{(A+\delta)^2-4B\delta}}{2B}. \tag{A33}$$

Using Eqs. (A5), (A11), and (A16), and using the fact that $r = 1$ in RCE, we can derive expressions for $M_{c,\mathrm{RCE}}$ and c_{RCE},

$$M_{c,\mathrm{RCE}} = -\frac{C}{Lq_v^*}Q, \tag{A34}$$

$$c_{\mathrm{RCE}} = -\frac{1}{L}Q, \tag{A35}$$

where

$$C = \left[A-\varepsilon-(B-\varepsilon)\frac{A+\delta-\sqrt{(A+\delta)^2-4B\delta}}{2B}\right]^{-1}. \tag{A36}$$

Using (10)–(13), which normalize the condensation rate and mass fluxes by RCE values, we can write Eqs. (A21)–(A27) as

$$\mathrm{RH} = \frac{-b_2-\sqrt{b_2^2-4b_1b_3}}{2b_1}, \tag{A37}$$

$$\gamma = A-B\mathrm{RH}, \tag{A38}$$

$$\Gamma = \frac{R_v T^2}{L}\left(A-B\mathrm{RH}+\frac{g}{R_a T}\right), \tag{A39}$$

$$r = \frac{\delta(1-\mathrm{RH})}{(A-B\mathrm{RH})\mathrm{RH}}, \tag{A40}$$

$$\tilde{c} = \frac{1}{r}, \tag{A41}$$

$$\tilde{M}_c = \frac{1}{Cr[\gamma-\varepsilon(1-\mathrm{RH})]}, \tag{A42}$$

$$\tilde{M}_e = \tilde{M}-\frac{1}{Cr[\gamma-\varepsilon(1-\mathrm{RH})]}, \tag{A43}$$

with variables

$$A = \frac{L}{R_v T^2}\frac{g\left(1+\frac{q_v^* L}{R_a T}\right)+q_v^* L\varepsilon}{c_p+\frac{q_v^* L^2}{R_v T^2}}-\frac{g}{R_a T}, \tag{A44}$$

$$B = \frac{L}{R_v T^2}\frac{q_v^* L\varepsilon}{c_p+\frac{q_v^* L^2}{R_v T^2}}, \tag{A45}$$

$$C = \left[A-\varepsilon-(B-\varepsilon)\frac{A+\delta-\sqrt{(A+\delta)^2-4B\delta}}{2B}\right]^{-1}, \tag{A46}$$

$$b_1 = \frac{B}{\delta}-C(\varepsilon-B)\tilde{M}, \tag{A47}$$

$$b_2 = -\frac{A+\delta}{\delta}-C(A+B-2\varepsilon)\tilde{M}, \tag{A48}$$

$$b_3 = 1-C(\varepsilon-A)\tilde{M}. \tag{A49}$$

This has eliminated Q from the solution.

REFERENCES

Becker, T., C. S. Bretherton, C. Hohenegger, and B. Stevens, 2018: Estimating bulk entrainment with unaggregated and aggregated convection. *Geophys. Res. Lett.*, **45**, 455–462, https://doi.org/10.1002/2017GL076640.

Bretherton, C. S., M. E. Peters, and L. E. Back, 2004: Relationships between water vapor path and precipitation over the tropical oceans. *J. Climate*, **17**, 1517–1528, https://doi.org/10.1175/1520-0442(2004)017<1517:RBWVPA>2.0.CO;2.

——, P. N. Blossey, and M. Khairoutdinov, 2005: An energy-balance analysis of deep convective self-aggregation above uniform SST. *J. Atmos. Sci.*, **62**, 4273–4292, https://doi.org/10.1175/JAS3614.1.

Durre, I., R. S. Vose, and D. B. Wuertz, 2006: Overview of the Integrated Global Radiosonde Archive. *J. Climate*, **19**, 53–68, https://doi.org/10.1175/JCLI3594.1.

Held, I. M., R. S. Hemler, and V. Ramaswamy, 1993: Radiative–convective equilibrium with explicit two-dimensional moist convection. *J. Atmos. Sci.*, **50**, 3909–3927, https://doi.org/10.1175/1520-0469(1993)050<3909:RCEWET>2.0.CO;2.

Jeevanjee, N., and D. M. Romps, 2018: Mean precipitation change from a deepening troposphere. *Proc. Natl. Acad. Sci. USA*, **115**, 11 465–11 470, https://doi.org/10.1073/pnas.1720683115.

Lawson, R. P., and W. A. Cooper, 1990: Performance of some airborne thermometers in clouds. *J. Atmos. Oceanic Technol.*, **7**, 480–494, https://doi.org/10.1175/1520-0426(1990)007<0480:POSATI>2.0.CO;2.

Mather, J. H., T. P. Ackerman, W. E. Clements, F. J. Barnes, M. D. Ivey, L. D. Hatfield, and R. M. Reynolds, 1998: An atmospheric radiation and cloud station in the tropical western Pacific. *Bull. Amer. Meteor. Soc.*, **79**, 627–642, https://doi.org/10.1175/1520-0477(1998)079<0627:AARACS>2.0.CO;2.

Po-Chedley, S., M. D. Zelinka, N. Jeevanjee, T. J. Thorsen, and B. D. Santer, 2019: Climatology explains intermodel spread in tropical upper tropospheric cloud and relative humidity response to greenhouse warming. *Geophys. Res. Lett.*, **46**, 13 399–13 409, https://doi.org/10.1029/2019GL084786.

Romps, D. M., 2010: A direct measure of entrainment. *J. Atmos. Sci.*, **67**, 1908–1927, https://doi.org/10.1175/2010JAS3371.1.

——, 2014: An analytical model for tropical relative humidity. *J. Climate*, **27**, 7432–7449, https://doi.org/10.1175/JCLI-D-14-00255.1.

——, 2016: Clausius–Clapeyron scaling of CAPE from analytical solutions to RCE. *J. Atmos. Sci.*, **73**, 3719–3737, https://doi.org/10.1175/JAS-D-15-0327.1.

——, 2020: *Fundamental Aspects of Turbulent Flows in Climate Dynamics*. Lecture Notes of the Les Houches Summer School, Vol. 109, Oxford University Press, 45 pp.

——, and A. B. Charn, 2015: Sticky thermals: Evidence for a dominant balance between buoyancy and drag in cloud updrafts. *J. Atmos. Sci.*, **72**, 2890–2901, https://doi.org/10.1175/JAS-D-15-0042.1.

Seeley, J. T., and D. M. Romps, 2015: Why does tropical convective available potential energy (CAPE) increase with warming? *Geophys. Res. Lett.*, **42**, 10 429–10 437, https://doi.org/10.1002/2015GL066199.

——, and ——, 2016: Tropical cloud buoyancy is the same in a world with or without ice. *Geophys. Res. Lett.*, **43**, 3572–3579, https://doi.org/10.1002/2016GL068583.

Sherwood, S. C., D. Hernandez-Deckers, M. Colin, and F. Robinson, 2013: Slippery thermals and the cumulus entrainment paradox. *J. Atmos. Sci.*, **70**, 2426–2442, https://doi.org/10.1175/JAS-D-12-0220.1.

Singh, M. S., and P. A. O'Gorman, 2013: Influence of entrainment on the thermal stratification in simulations of radiative-convective equilibrium. *Geophys. Res. Lett.*, **40**, 4398–4403, https://doi.org/10.1002/grl.50796.

——, Z. Kuang, E. D. Maloney, W. M. Hannah, and B. O. Wolding, 2017: Increasing potential for intense tropical and subtropical thunderstorms under global warming. *Proc. Natl. Acad. Sci. USA*, **114**, 11 657–11 662, https://doi.org/10.1073/pnas.1707603114.

——, R. A. Warren, and C. Jakob, 2019: A steady-state model for the relationship between humidity, instability, and precipitation in the tropics. *J. Adv. Model. Earth Syst.*, **11**, 3973–3994, https://doi.org/10.1029/2019MS001686.

Warren, R. A., M. S. Singh, and C. Jakob, 2020: Simulations of radiative-convective-dynamical equilibrium. *J. Adv. Model. Earth Syst.*, **12**, e2019MS001734, https://doi.org/10.1029/2019MS001734.

Wing, A. A., and T. W. Cronin, 2016: Self-aggregation of convection in long channel geometry. *Quart. J. Roy. Meteor. Soc.*, **142**, 1–15, https://doi.org/10.1002/qj.2628.

——, K. Emanuel, C. E. Holloway, and C. Muller, 2017: Convective self-aggregation in numerical simulations: A review. *Surv. Geophys.*, **38**, 1173–1197, https://doi.org/10.1007/s10712-017-9408-4.